Computational Materials Science 92 (2014) 457–463

Contents lists available at ScienceDirect

Computational Materials Science

journal homepage: www.elsevier.com/locate/commatsci

Atomistic simulation of soldering iron filled carbon nanotubes

Vicente Munizaga [a,b], Griselda García [a,b], Eduardo Bringa [c], Mariana Weissmann [d], Ricardo Ramírez [a,b], Miguel Kiwi [b,e,*]

[a] Facultad de Física, Universidad Católica de Chile, Casilla 306, Santiago 7820436, Chile
[b] Centro para el Desarrollo de la Nanociencias y Nanotecnología, CEDENNA, Avenida Ecuador 3493, Santiago, Chile
[c] CONICET and Facultad de Ciencias Exactas y Naturales, Universidad Nacional de Cuyo, Mendoza 5500, Argentina
[d] Departamento de Física, Comisión Nacional de Energía Atómica, Avda. del Libertador 8250, (1429) Buenos Aires, Argentina
[e] Departamento de Física, Facultad de Ciencias, Universidad de Chile, Casilla 653, Santiago 7800024, Chile

ARTICLE INFO

Article history:
Received 12 February 2014
Received in revised form 30 April 2014
Accepted 5 June 2014

Keywords:
Iron filled carbon nanotubes
Nanotube soldering
Structure optimization
Molecular dynamics

ABSTRACT

The melting and soldering processes of two iron filled carbon nanotubes is explored by means of classical molecular dynamics, in order to develop an understanding of the underlying mechanisms that govern the dynamics of nano-soldering. Molten Fe flows from the open end of the two CNTs, leading to a liquid junction, and eventually to a solid contact. This soldering process is accompanied by partial or total healing of the carbon nanotubes, which after cooling and relaxation form just a single unit which encapsulates the iron, depending on the relative separation, diameters and axial offset of the nanotubes. This makes for a promising scenario for CNT soldering, repairing and healing, and a variety of different tools in the field of nanoelectronics.

1. Introduction

For some time, carbon nanotubes (CNTs) have been the focus of extensive research for physicists, chemists and applied scientists, due to their interest to basic science and because of their various potential and current technological applications. These applications encompass areas as diverse as body-armor, fibers with high tensile strength, logic circuits with CNT transistors [1], inter- and intramolecular logic gates [2], highly bendable transparent thin-film transistors that use CNT based conductors and semiconductors with elastomeric dielectrics [3], etc.

The metal catalyzed nucleation and growth mechanism of CNT has been investigated experimentally [4–6] and simulated theoretically [7,8]. Moreover, the feasibility of fabricating hetero-junctions between metals and CNTs has also been explored [9]. In particular iron-filled CNTs pose an interesting challenge from a basic viewpoint, underlined by the application they have found as magnetic force microscopy probes [10–13], and their potential in the synthesis of nanoparticles [14]. Mechanical properties of Fe filled CNTs were recently simulated for different Fe cores using quasi-static simulations [15], and in general, metal filled CNTs have aroused research interest because of their applicability as very-large-scale integration interconnects due to their high thermal stability, large thermal conductivity and current carrying capacity. Thus, the potential for the use of an Fe filled CNT as a nanoscale soldering device is a subject of special interest. The latter was recently implemented experimentally by Misra and Daraio [16]. They found that two multi-wall CNTs separated by only a few nanometers, were joined by the out-flowing Fe, molten by electron bombardment. In this contribution to metal-filled CNT research we explore, by means of classical molecular dynamics, the melting process and the soldering of two iron filled CNT, for a variety of different scenarios. Kashiwase et al., around the same time, reported soldering nanotubes using an atomic force microscope [17], but this was achieved differently. They used an iron oxide nanoparticle, instead of a nanowire, to join two or more CNTs from the outside.

Very recently a paper by Cui et al. [18] reported simulations, closely related to ours, in which a Ag nanoparticle is employed to solder two fixed axially positioned single-walled CNTs on a silicon surface. In spite of the fact that their model is quite different (they use a metal drop to solder, while we start with a metal filled CNT), it is remarkable that the system evolution and the final configurations are similar.

* Corresponding author at: Depto. de Física, Facultad de Ciencias, Universidad de Chile, Casilla 653, Santiago 7800024, Chile. Tel.: +56 2 2978 7290; fax: +56 2 2271 2973.
E-mail address: m.kiwi.t@gmail.com (M. Kiwi).

http://dx.doi.org/10.1016/j.commatsci.2014.06.006
0927-0256/

2. Model

Here we report on simulation results of how two iron filled CNTs subject to a temperature cycle interact and solder. Several cases are investigated: (i) two coaxial (18,18) CNTs closed on one end and filled with (0 0 1) bcc Fe, initially less than 2 nm apart; (ii) two coaxial (18,18) CNTs closed on one end and filled with (1 1 0) bcc Fe, initially less than 2 nm apart; (iii) two non-coaxial (18,18) CNTs closed on one end, and filled with (1 1 0) bcc Fe, initially less than 2.2 nm apart; (iv) two open ended coaxial (18,18) CNTs, with their position fixed in space and filled with (1 1 0) bcc Fe; (v) two open ended non-coaxial (18,18) CNTs, with their position fixed in space and filled with (1 1 0) bcc Fe; (vi) two closed on one end and filled with (1 1 0) bcc Fe, coaxial CNTs of different diameter, that is one (18,18) and another (29,29); and (vii) two closed on one end and filled with (1 1 0) bcc Fe, non- coaxial CNTs of different diameter, that is one (18,18) and another (29,29).

We generated a capped (18,18) CNT, with a diameter of 2.37 nm, and a length of 5.40 nm along the z-axis. The CNT was filled with a single crystal cylinder of bcc Fe (diameter 1.63 nm and length 5.11 nm), oriented either along the [0 0 1] or the [1 1 0] direction along the CNT axis, and extending up to the rim of the nanotube. We duplicate this configuration to create a mirror image second CNT, either aligned or axially offset parallel to the former along the z axis, with their opposite open ends separated by a 2 nm gap as illustrated in Fig. 1a, in which the Fe is oriented with the [0 0 1] direction parallel to the CNT axis. This implies a total of 3528 carbon and 2400 iron atoms, for a total of 5928 atoms. We followed the evolution of this system under heating, to mimic the effect of an electron beam, using molecular dynamics. MD simulations were run with LAMMPS [19]. For the C–C interactions we used the AIREBO potential [20] with a cut-off of 1.0 nm and neglecting torsional contributions. A CNT simulated with this potential is stable and does not expand significantly up to temperatures well above the bulk Fe melting temperature. For the Fe–Fe interactions we used the EAM potential by Mendelev et al. [21], while the Fe–C interactions were simulated with the Lennard–Jones potential as used by Banerjee et al. [8].

There are many interaction potentials for Fe–C, starting with the classical fit by Johnson [22]. However, they are typically meant to describe C as an impurity in Fe and, therefore, greatly overestimate the binding between Fe and the C of the CNT wall. The recent work by Lee [23] using MEAM potentials might help with this problem. However, in this paper we chose the simple potential by Banerjee et al. [8], since it provides appropriate binding energies for Fe inside the NT, and is computationally very efficient.

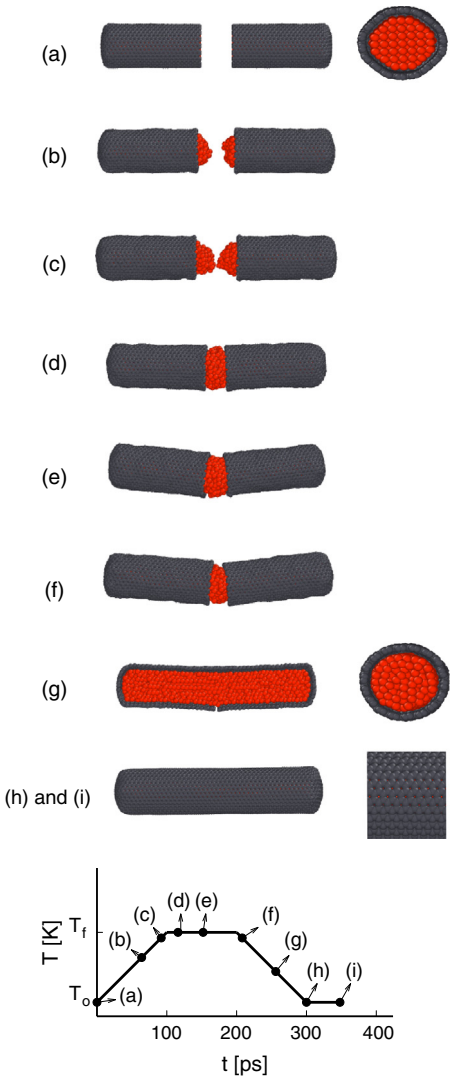

Fig. 1. Snapshots of the soldering process of two iron filled (18,18) CNTs. Initially ($t = 0$) the Fe [0 0 1] direction is parallel to the CNT axis, as illustrated by the frontal view. Initial temperature $T_0 = 10$ K, maximum temperature $T_f = 2000$ K, and temperature ramp rise time $t_r = 100$ ps. The temperature and simulation time of each of the snapshots is given by the ramp displayed at the bottom of the figure. Some images are sliced to show the inner Fe structure. The images to the right in (a) and (g) correspond to cuts perpendicular to the CNT axis. The image to the right of (h) and (i) zooms in on the region where the CNTs have coalesced, and reveals the completion of the healing process. The system consists of 3528 Fe (red) and 2400 C (gray) atoms. (For interpretation of the references to color in this figure legend, the reader is referred to the web version of this article.)

3. Results

In order to mimic the heating by an electron beam, which was rastered during the experiment, we applied a temperature ramp to the whole system, as is usually done in ion-induced thermal spike simulations [24]. As illustrated at the bottom of Fig. 1 the temperature was increased from T_0 = 10 K (Fig. 1a) to $T_f = 2000$ K, using a linear ramp during $t_r = 100$ ps, in time steps of 1 fs. Next the temperature was kept at T_f during a time t_r, and then lowered back to T_0 following a linear temperature ramp during an additional time t_r. Finally, T was kept at 10 K during $t_r/2$. We also varied T_f from 1500 to 3000 K, and t_r was varied from 10 ps to 10 ns; the final results turned out to be insensitive to all these changes of the molecular dynamics simulations. The Fe melting temperature T_f, as computed for the Fe potential used from phase coexistence simulations [25,26], turns out to be larger than the bulk Fe melting temperature (1772 K). As a matter of fact the precise determination of the melting T constitutes a challenging problem. Several different methods to calculate T_f, other than phase coexistence, have been reported, like the one put forward by Weingarten et al. [27], which focuses on the hysteresis of the melting-solidification process, and a potential energy versus T based procedure by Cui et al. [18]. However, for our investigation, the precise determination of the absolute value of T_f is not the main objective, since the actual melting point for nanoparticles in atomistic simulations strongly depends on heating rate, system size, etc. [25]. Nevertheless, our "melting temperature" gives a reasonable estimate for the threshold temperature at which the Fe nanowire starts flowing out of the CNT.

Liquid flow is observed towards the open ends of the CNTs (Fig. 1b and c) and a contact is established between both ends of the CNTs, mediated by the liquid Fe, as shown in Figs. 1d and e. In Fig. 1f a contact between the two CNTs is established,

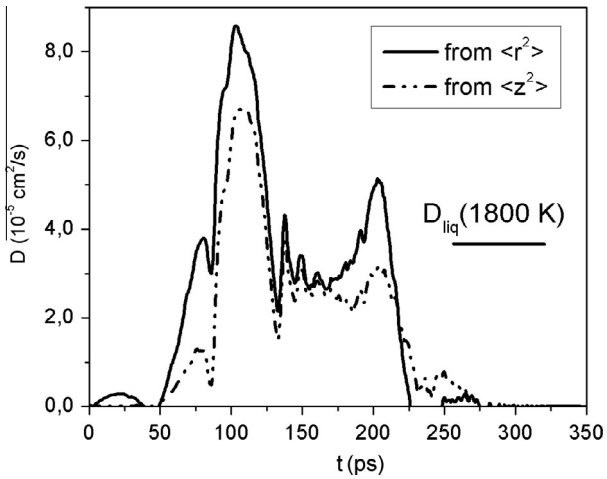

Fig. 2. Fe diffusivity versus time for the process illustrated in Fig. 1, including partial diffusivity due only to axial motion (along z). As a reference, the equilibrium diffusivity of liquid Fe at 1800 K is also shown.

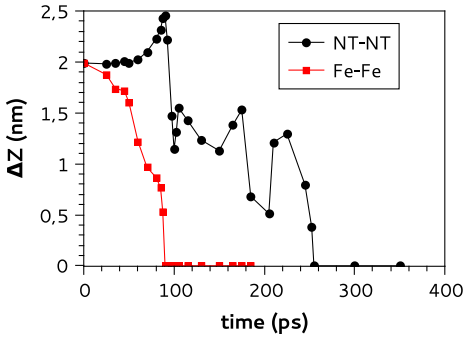

Fig. 3. Gap Δz between the Fe nanowires (red squares), and the CNTs (black circles), for the process illustrated in Fig. 1. $T_f = 2000$ K, $t_r = 100$ ps. It is noticed that, because the center of mass remains fixed, the CNTs separate until the Fe nanowires establish contact. Thereafter the CNTs go through a rearrangement process until, at ≈ 255 ps, the healing is completed. The iron nanowires relative speed is evaluated as dz/dt, and yields a value of 5–80 m/s. The Fe gap was calculated on the basis of the shortest distance between atoms on both sides. The CNT gap was estimated averaging the C–C distances. (For interpretation of the references to color in this figure legend, the reader is referred to the web version of this article.)

accompanied by a mismatch between the axial direction of the two NT's. Upon cooling the formation of the contact is driven by a large diffusivity along the NT axis, and finally a healing of the CNT into a single continuous structure is observed in Fig. 1h and i when the system reaches 10 K. When the same procedure is applied to the two bare (non-encapsulated) Fe single crystal cylinders, separated by the same 2 nm gap, they simply form two separate quasi spherical iron clusters.

The diffusivity along the NT symmetry z-axis, which corresponds to the slope of the mean square displacement versus time [28], is displayed in Fig. 2. The contribution to the total diffusivity from the z-component is large, indicating transport along the CNT axis. The bar in Fig. 2 indicates the reported diffusivity of the liquid [21]. There is a transition from solid to liquid at $T \approx 1800$ K, and the diffusivity obtained from this data is $\sim 3\ \mathrm{cm}^2/\mathrm{s}$, which compares well with the value $3.6\ \mathrm{cm}^2/\mathrm{s}$ reported for this potential [21]. However, the peak diffusivity around the Fe contact formation time is 3 times larger. The formation of a liquid was also confirmed by examination of the Fe pair correlation function. The liquid flows at 10–80 m/s, which is similar to the velocity (20 m/s) for the flow of water through sub-micrometer-thick membranes, made of graphene oxide, reported by Nair et al. [29].

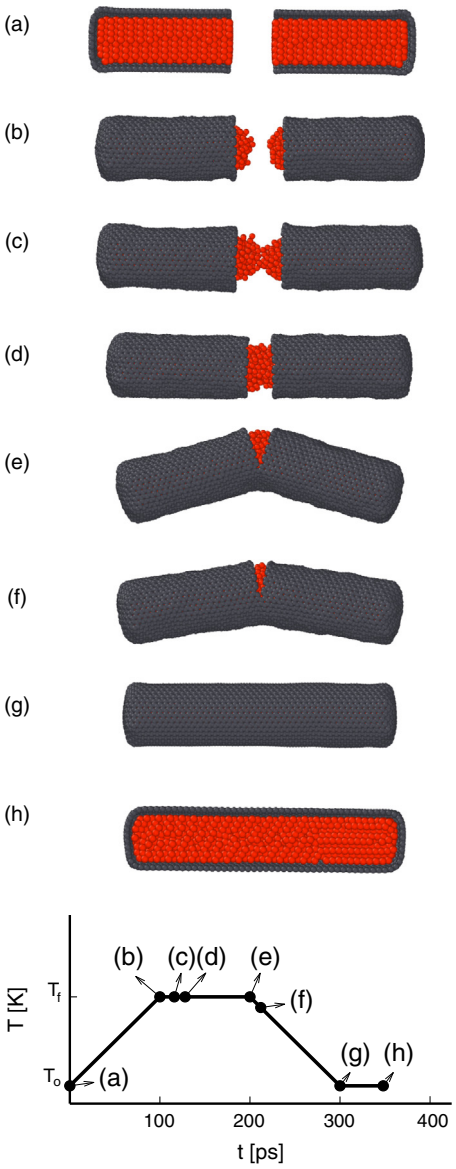

Fig. 4. Snapshots of the soldering process of iron filled (18,18) CNTs. Initially ($t = 0$) the Fe [1 1 0] direction is parallel to the CNT axis. The temperature and simulation time of each of the snapshots is given by the ramp displayed at the bottom of the figure. The system consists of 3526 Fe (red) and 2520 C (gray) atoms. (For interpretation of the references to color in this figure legend, the reader is referred to the web version of this article.)

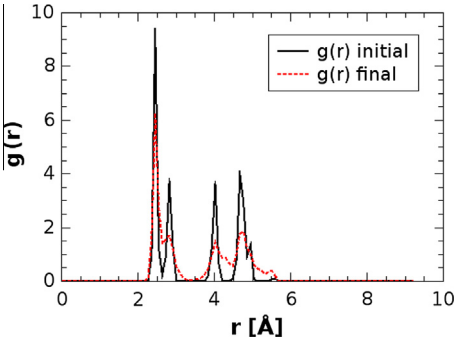

Fig. 5. Iron radial distribution function $g(r)$ for the initial (continuous black) and final (dashed red) configurations for Fig. 4. (For interpretation of the references to color in this figure legend, the reader is referred to the web version of this article.)

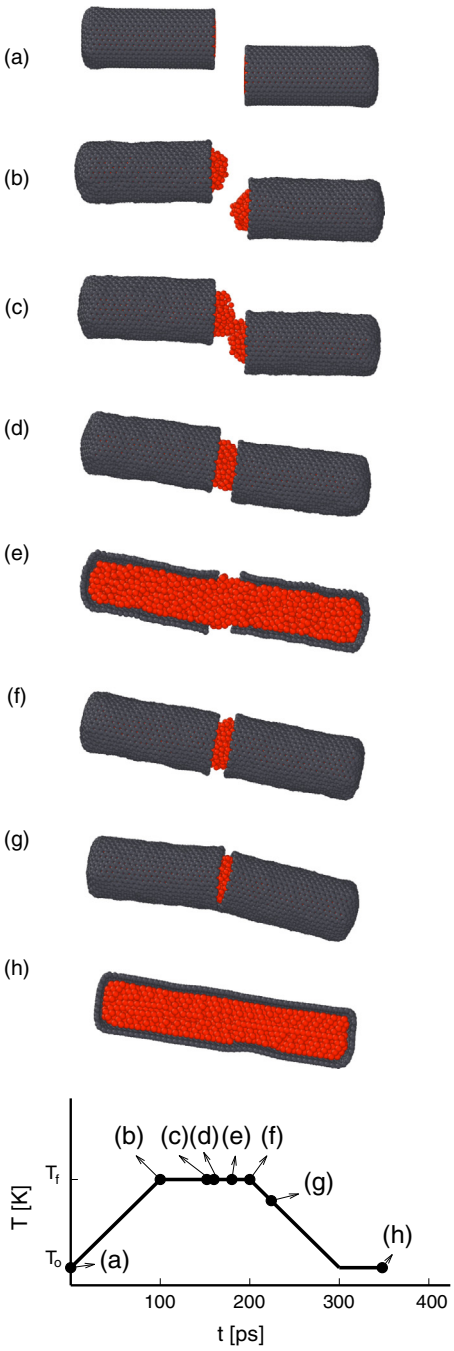

Fig. 6. Snapshots of two iron filled (18,18) CNTs that initially are longitudinally separated by 1.5 nm and whose parallel axis are perpendicularly displaced by 1.55 nm. Initially ($t = 0$) the Fe [1 1 0] direction is parallel to the CNT axis. The temperature and simulation time of each of the snapshots is given by the ramp displayed at the bottom of the figure.

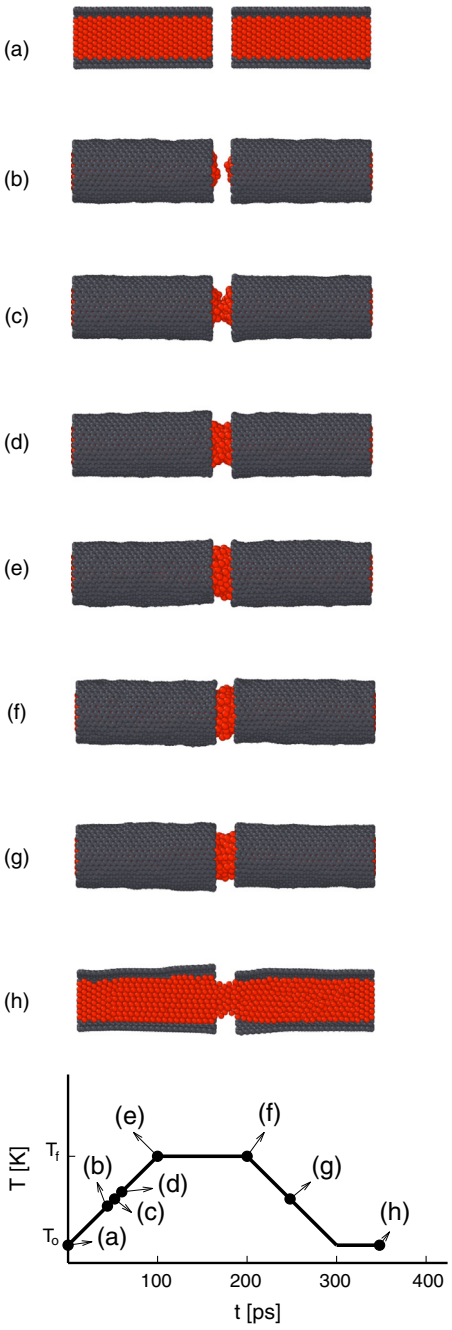

Fig. 7. Snapshots of two open ended iron filled (18,18) CNTs, whose two first Fe and C layers at the left and right ends are kept clamped. Initially ($t = 0$) the Fe [1 1 0] direction is parallel to the CNT axis. The initial gap between the CNTs is 1 nm. The temperature and simulation time of each of the snapshots is given by the ramp displayed at the bottom of the figure. The system consists of 3384 Fe (red) and 2578 C (gray) atoms. (For interpretation of the references to color in this figure legend, the reader is referred to the web version of this article.)

Fig. 3 shows the gap between the CNTs and also the length of the Fe outflow from the CNT rim (averaged over both CNTs). It can be seen that, as the system is cooled down the Fe atoms start to solidify and contract (Figs. 1 and 3), which is also apparent by the decrease in diffusivity in Fig. 2. This contraction pulls the previously separated rims of the CNTs together, forming a junction which can be seen in Fig. 1d–g. The pair correlation function of the Fe inside the NT shows that it crystallizes into the bcc structure, but including defects, as expected from the rapid re-crystallization as recently discussed by Jiang et al. [30] and observed in Fig. 1h. The inner part of the Fe core has a binding energy close to the perfect bulk bcc binding for this potential.

We simulated the same process described above, just changing the orientation of the Fe filling, by aligning the CNT axis with the Fe [1 1 0] direction, as illustrated in Fig. 4. When Fig. 4 is compared with Fig. 1 it is apparent that the crystallographic direction that is adopted plays only minor role in the soldering process. Also the radial distribution function and the diffusivity, which are discussed later on, do not exhibit significant dependence on the crystal orientation. Therefore, in what follows, we limit our attention to

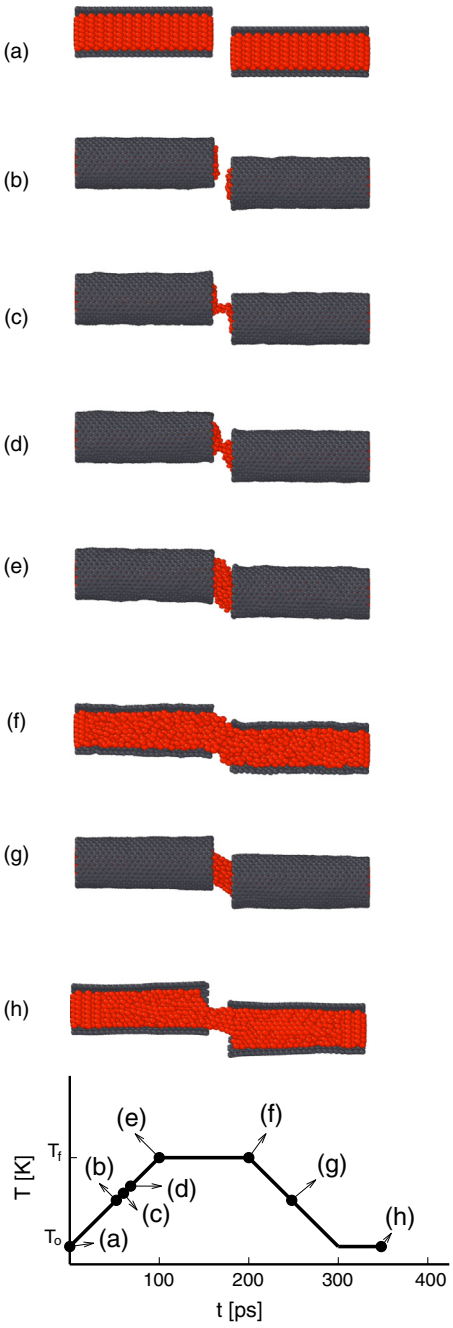

Fig. 8. Snapshots of two open ended iron filled (18,18) CNTs, whose two first Fe and C layers at the left and right ends are kept clamped. Initially ($t = 0$) the Fe [1 1 0] direction is parallel to the CNT axis, and each time step is 1 fs. The initial gap between the CNTs and the perpendicular displacement are of 1 nm.The temperature and simulation time of each of the snapshots is given by the ramp displayed at the bottom of the figure. The system consists of 3384 Fe (red) and 2578 C (gray) atoms. (For interpretation of the references to color in this figure legend, the reader is referred to the web version of this article.)

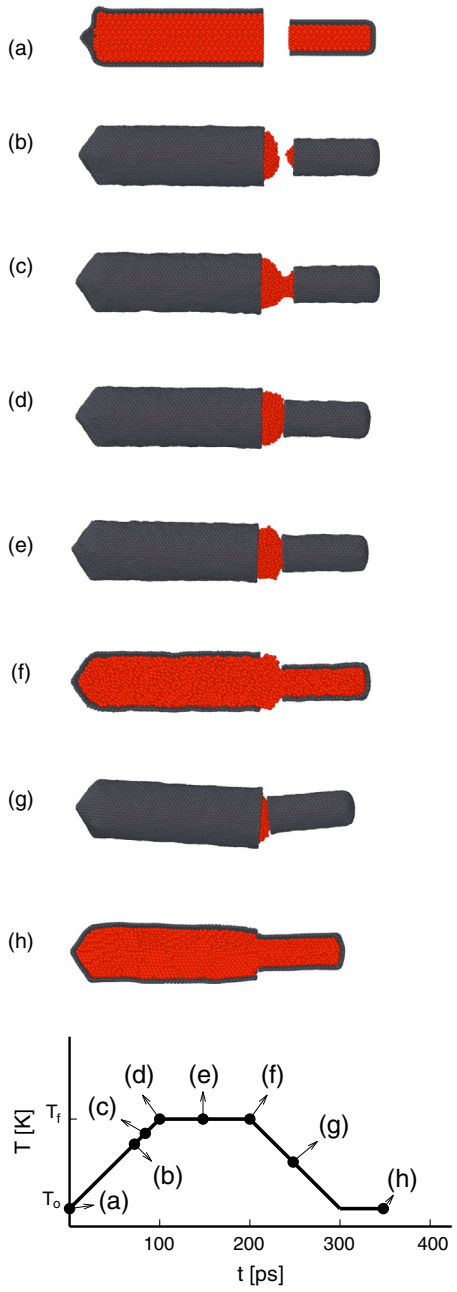

Fig. 9. Snapshots of open ended iron filled (18,18) and (29,29) CNTs. Initially ($t = 0$) the Fe [1 1 0] direction is parallel to the CNT axis. The C diameter is 2.40 nm and its length 5.55 nm. The initial gap between the CNTs is 1.89 nm. The (29,29) CNT diameter is 2.40 nm and its length 5.55 nm, and its inner Fe diameter and length are 1.64 and 5.54 nm, respectively. The temperature and simulation time of each of the snapshots is given by the ramp displayed at the bottom of the figure. The system consists of 3384 Fe (red) and 2578 C (gray) atoms. (For interpretation of the references to color in this figure legend, the reader is referred to the web version of this article.)

CNTs filled with Fe [1 1 0]. Mechanical properties of Fe nanowires do depend on Fe orientation [15]. However, the Fe nanowire melting only depends very weakly on orientation, as can be seen by inspection of Fig. 1, which illustrates the simulations we carried out for the [001] orientation which, as expected, show similar features when compared with the [1 1 0] results for the process under investigation, that are reported below.

Additional information of interest is provided by the iron radial distribution function $g(r)$, which is shown in Fig. 5, where we notice that the ordered initial structure (black continuous line) is not greatly altered when the final Fe configuration is reached, at the end of the cooling process. In other words, much of the Fe remains bcc ordered.

It is relevant to find out how robust the soldering process is against misalignment of the CNTs. In Fig. 6 we illustrate the soldering of two CNT that initially have their parallel symmetry axis displaced by 1.55 nm. The initial longitudinal gap is of 1.5 nm. It is quite apparent that the soldering and healing processes are able to withstand a significant perpendicular displacement of the axis.

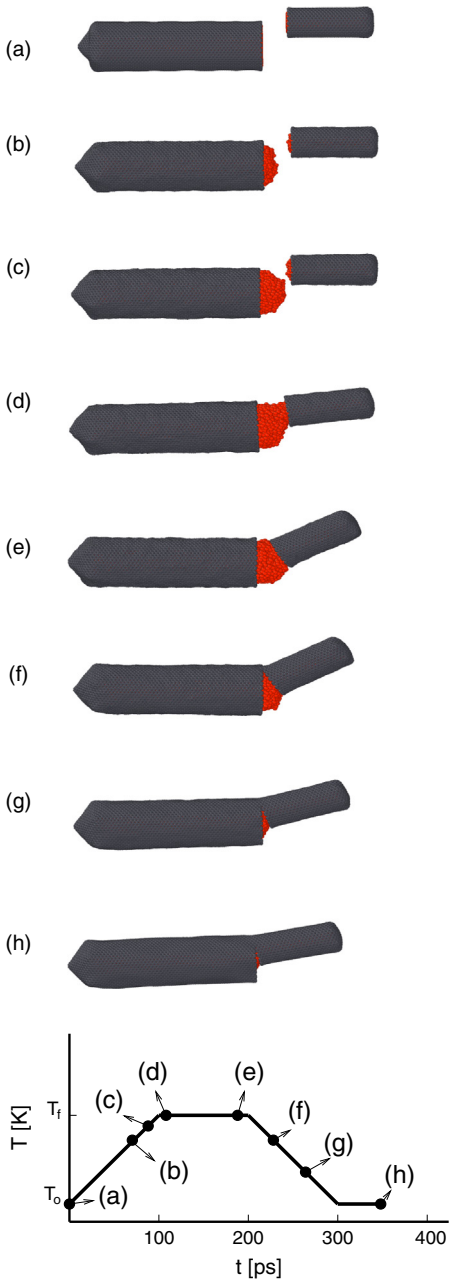

Fig. 10. Snapshots of open ended axially displaced iron filled (18,18) and (29,29) CNTs. Initially ($t = 0$) the Fe [1 1 0] direction is parallel to the CNT axis. The initial gap between the CNTs is 1.89 nm and their axis are displaced by 2 nm. The inner Fe and C diameters are 1.642 and 3.25 nm, and the C ones are 2.4 and 4.00 nm. The inner Fe lengths are 5.54 and 10.6 nm, and the CNTs are 5.55 and 12.2 nm long. The temperature and simulation time of each of the snapshots is given by the ramp displayed at the bottom of the figure. The system consists 10 194 Fe (red) and 7 794 C (gray) atoms. (For interpretation of the references to color in this figure legend, the reader is referred to the web version of this article.)

Fig. 11. Illustration of how two open ended misaligned different diameter iron filled CNTs stick together at the end (stage *h* of Fig. 10) of the soldering process shown in detail in Fig. 10.

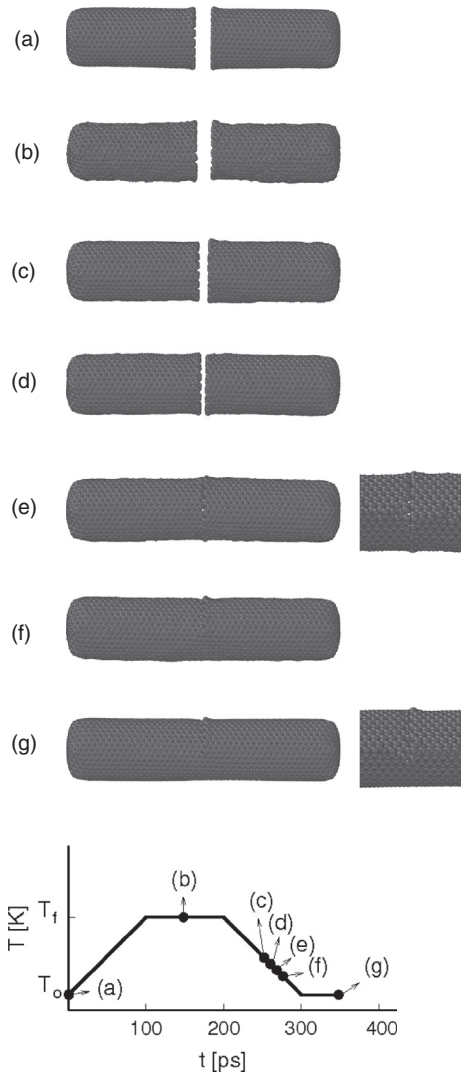

Fig. 12. Illustration of the sequence of how two open ended aligned empty CNTs stick together. The initial gap between the CNTs is ~ 2 nm. We remark that the bonding process does not start until the gap between the CNTs is reduced to 0.83 nm. On the right hand side of (e) and (g) we enlarge the contact region to better display the defects that appear.

Another important feature is how clamping the CNTs affects soldering. In Fig. 7 we illustrate what happens when we carry out the process for two open-ended Fe filled and clamped CNTs. Here the two first Fe and C layers on the extreme left and right of the CNTs illustrated in Fig. 7 are kept fixed in space and frozen (with no dynamics). The soldering process certainly does change, in that the Fe contact area at the open ends of the CNT acquire a significantly smaller diameter, but nevertheless it achieves full completion. When the axis of the same clamped CNT are displaced perpendicular to their long axis something quite similar occurs, as illustrated in Fig. 8. This underscores the relation of our results with the ones recently reported by Cui et al. [18], on a different system and with a different soldering material. In fact, the support of the nanotubes on a Si substrate, in the calculations by Cui et al., effectively acts as a CNT clamping mechanism.

Experimentally one cannot expect that the CNTs available are all of the same diameter. Therefore, it is also of interest to

determine what happens in that case. In Fig. 9 we can observe that the soldering process does complete, in spite of the significant diameter difference.

We also illustrate the process when two different diameter axially offset CNTs are investigated. The results are provided in Fig. 10, where we observe that not only they do solder, but that there is a tendency for the CNTs to stick together as well. Additional insight is provided by Fig. 11 where an axial view of the final stage of the process is provided.

Finally, we simulate the case of two CNTs without Fe filling, which is illustrated in Fig. 12. In this case we reduce the gap, starting from a C–C distance of ~2 nm, which is larger than the potential cut-off of 1.0 nm, and nothing much happens until it is diminished to 0.83 nm, at which point the bonding starts. The computations were performed in two different ways: (i) first we started from a configuration where one CNT was the mirror image of the other; and, (ii) next we slightly rotated the second CNT to achieve a better bond matching among them (fitting hexagons). Both computations led to similar final configurations, and we observe that the welding is not perfect, in contrast with what happens to Fe filled CNTs.

Experiments have been carried out for multiwall CNTs, instead of SW-CNTs. Additional walls, as in the case of the nanocages treated by Sun et al. [31] would increase the confinement effect and allow for larger liquid flow, as reported by Misra and Daraio [16] for larger MW-CNTs. The Fe–C interaction used here is not adequate when defects are present or at the CNT rim. However, for CNTs wide enough, this might not affect significantly the Fe outflow. We expect that CNTs filled with other metals, which in general have a larger solidification shrinkage than Fe (3.16%), like Al (7.14%), Au (5.47%), Co (5.26%), Cu (5.3%) and Ni (5.11%), to behave similarly.

4. Conclusion

In summary, we have simulated the formation of CNT-metal contacts using molecular dynamics simulations. Our results are in qualitative agreement with the experiments reported by Misra and Daraio [16], and we found that they constitute a possible tool to repair CNT break-ups in future CNT-based nanoelectronic devices. We anticipate that a large droplet of Fe on top of a CNT might prevent the closure of the CNT contact, but allow CNT multi-junctions [32]. Moreover, CNT-metal contacts in general might be useful for the repair and stabilization of nanowire circuits, as recently demonstrated by Illie et al. [33], and in general, for a variety of different uses in the field of nanoelectronics [1–3]. According to our classical simulations, the final metallic structure includes relatively few defects, and its conductivity should not be severely affected. It remains to test the mechanical properties of these junctions, but given the extensive repair observed here, they should be able to withstand significant stress.

Acknowledgments

This work was supported by the Fondo Nacional de Investigaciones Científicas y Tecnológicas (FONDECYT, Chile) under grants #1080239 and 1110630 (GG and RR), #1120399 and #1130272 (MK), and Financiamiento Basal para Centros Científicos y Tecnológicos de Excelencia (GG, MK and RR). E.M.B. thanks funding through grant PICT2009-0092 from the Agencia Nacional de Investigaciones Científicas, Argentina, and from the SeCTyP, U.N. Cuyo.

References

[1] A. Bachthold, P. Hadley, T. Nakanishi, C. Dekker, Science 294 (2001) 1317.
[2] V. Derycke, R. Martel, J. Appenzeller, P. Avouris, Nanoletters 1 (2001) 453.
[3] Q. Cao, S.H. Hur, Z.T. Zhu, Y. Sun, C. Wang, M.A. Meitl, M. Shim, J.A. Rogers, Adv. Mat. 18 (2006) 304.
[4] C.P. Deck, K. Vecchio, Carbon 44 (2006) 267.
[5] Y. Homma, Y. Kobayashi, T. Ogino, D. Takagi, R. Ito, Y.J. Jung, P.M. Ajayan, J. Chem. Phys. B 107 (2003) 12161.
[6] H. Yoshida, S. Takeda, T. Uchiyama, H. Kohno, Y. Homma, Nanoletters 8 (2008) 2082.
[7] F. Ding, K. Bolton, A. Rosén, J. Phys. Chem. B 108 (2004) 17369.
[8] S. Banerjee, S. Naha, I.K. Puri, Appl. Phys. Lett. 92 (2008) 233121.
[9] J.A. Rodríguez-Manzo, A. Tolvanen, A.V. Krasheninnikov, K. Nordlund, A. Demortière, F. Banhart, Nanoscale 2 (2010) 901.
[10] A. Winkler, T. Mühl, S. Menzel, R. Kozhuharova-Koseva, S. Hampel, A. Leonhardt, B. Büchner, J. Appl. Phys. 99 (2006) 104905.
[11] F. Wolny, U. Weissker, T. Mühl, A. Leonhardt, S. Menzel, A. Winkler, B. Büchner, J. Appl. Phys. 104 (2008) 064908.
[12] F. Wolny, T. Mühl, U. Weissker, A. Leonhardt, U. Wolff, D. Givord, B. Büchner, J. Appl. Phys. 108 (2010) 013908.
[13] F. Wolny, T. Mühl, U. Weissker, K. Lipert, J. Schumann, A. Leonhardt, B. Büchner, Nanotechnology 21 (2010) 435501.
[14] S. Coh, W. Gannett, A. Zettl, M.L. Cohen, S.G. Louie, Phys. Rev. Lett. 110 (2013) 185901. <http://link.aps.org/doi/10.1103/PhysRevLett.110.185901>.
[15] G. Soldano, M.M. Mariscal, Nanotechnology 20 (2009) 165705.
[16] A. Misra, C. Daraio, Adv. Mat. 20 (2008) 1.
[17] Y. Kashiwase, T. Ikeda, T. Oya, T. Ogino, Appl. Surface Sci. 254 (2008) 7897.
[18] J. Cui, L. Yang, L. Zhou, Y. Wang, ACS Appl. Mater. Interfaces 6 (2014) 2044.
[19] S.J. Plimpton, J. Comp. Phys. 117 (1995) 1. http://lammps.sandia.gov.
[20] S.J. Stuart, A.B. Tutein, J.A. Harrison, J. Chem. Phys. 112 (2000) 6472.
[21] M.I. Mendelev, S. Han, D.J. Srolovitz, G.J. Ackland, D.Y. Sun, M. Asta, Phil. Mag. 83 (2003) 3977.
[22] R.A. Johnson, Phys. Rev. 134 (1964) A1329.
[23] B.-J. Lee, Acta Mater. 54 (2006) 701.
[24] E.M. Bringa, R.E. Johnson, Phys. Rev. Lett. 88 (2002) 165501.
[25] S.-N. Luo, T.J. Ahrens, T. Çağin, A. Strachan, W.A. Goddard, D.C. Swift, Phys. Rev. B 68 (2003) 134206. <http://link.aps.org/doi/10.1103/PhysRevB.68.134206>.
[26] Z. Lin, E. Leveugle, E.M. Bringa, L.V. Zhigilei, Jour. Phys. Chem. C 114 (2010) 5686.
[27] N.S. Weingarten, W.D. Mattson, B.M. Rice, J. Appl, Phys. 106 (2006) 063524.
[28] M.I. Mendelev, Physics B 262 (1999) 40.
[29] R.R. Nair, H.A. Wu, P.N. Jayaraman, I. Grigorieva, A.K. Geim, Science 335 (2012) 442.
[30] Y.Y. Jiang, K. Zhang, H.Q. Yu, Y.Z. He, X.G. Song, Eur. Phys. Lett. 97 (2012) 16002.
[31] L. Sun, A.V. Krasheninnikov, T. Ahlgren, K. Nordlund, F. Banhart, Phys. Rev. Lett. 101 (2008) 156101.
[32] J.A. Rodríguez-Manzo, M. Wang, F. Banhart, Y. Bando, D. Golberg, Adv. Mater. 21 (2009) 4477.
[33] A. Illie, S. Crampin, L. Karlsson, M. Wilson, Nano Res. 5 (2012) 833.